

Efficient First-Principles Approach with a Pseudohybrid Density Functional for Extended Hubbard Interactions

Sang-Hoon Lee* and Young-Woo Son†
Korea Institute for Advanced Study, Seoul 02455, Korea

For massive database-driven materials research, there are increasing demands for both fast and accurate quantum mechanical computational tools. Contemporary density functional theory (DFT) methods can be fast sacrificing their accuracy or be precise consuming a significant amount of resources. Here, to overcome such a problem, we present a DFT method that exploits self-consistent determinations of the on-site and inter-site Hubbard interactions (U and V) simultaneously and obtain band gaps of diverse materials in the accuracy of GW method at a standard DFT computational cost. To achieve self-consistent evaluation of U and V , we adapt a recently proposed Agapito-Curtarolo-Buongiorno Nardelli pseudohybrid functional for U to implement a new density functional of V . This method is found to be appropriate for considering various interactions such as local Coulomb repulsion, covalent hybridization and their coexistence. We also obtained good agreements between computed and measured band gaps of low dimensional systems, thus meriting the new approach for large-scale as well as high throughput calculations for various bulk and nanoscale materials with higher accuracy.

I. INTRODUCTION

Theoretical and computational methods based on the density functional theory (DFT) [1, 2] have been indispensable tools in understanding physical properties of real materials [3]. Although they fail quantitatively and sometimes qualitatively in calculating band gaps [3] with the local density approximation (LDA) [2] or the generalized-gradient approximation (GGA) [4], they are only currently available methods without significant computational costs to offer fully quantum mechanical computational results for diverse phenomena involved with many thousands of electrons [3, 5]. Thus, regardless of such shortcomings, the DFT-based approaches prevail in data-driven materials researches [6] spanning various areas such as energy materials [7–9], electronic applications [10–12], low dimensional crystals [13] and topological materials [14–17]. These databases with improved accuracy will be of great benefit in advancing future technology.

To build high-quality materials databases, it is vital to improve the accuracy of DFT-based methods. Several methods beyond LDA and GGA have been suggested so far. The local Coulomb repulsion U was introduced in DFT+ U to compensate the overdelocalization of d - or f -electrons in LDA or GGA [18, 19]. Beyond static correlation effectively treated in DFT+ U , DFT with the dynamical mean-field theory [20–22] has been used for strongly interacting materials. The quasiparticle energy of semiconductors can be obtained accurately with the GW approximations [23–25]. Hybrid functionals such as HSE [26, 27] and LDA with the modified Becke-Johnson exchange potential (mBJLDA) [28] are also popular. However, all the methods above except DFT+ U

and mBJLDA involves intensive computations discouraging their use in data-driven researches. Due to some limitations in the latter [29], we will focus on improving the former for high-throughput calculations.

Two aspects in the DFT+ U formalism are important in obtaining accurate band gaps *ab initio*. First, the on-site Hubbard U needs to be estimated self-consistently [30] and various methods for this purpose [30–37] have been suggested. Among them, the direct evaluation from the Hartree-Fock (HF) formalism [35–37] is relevant here since other methods involve additional expensive calculations. A recent proposal by Agapito-Curtarolo-Buongiorno Nardelli (ACBN0) [37] allows a direct self-consistent evaluation of U . They demonstrated improved agreements with experiments with a negligible increase in computational cost [37, 38]. Second, the inter-site Hubbard V between the localized orbital of interest in DFT+ U and its neighboring orbitals also need to be considered properly because it could lead to better descriptions of electronic structures of some solids [39–41]. Moreover, DFT+ U hardly improves LDA and GGA gaps of simple semiconductors such as Si while DFT+ U with V does [40]. Therefore, by combining these progresses, we may obtain an efficient large-scale and high-throughput computational tool for materials researches.

In this paper, we extend the ACBN0 functional for DFT+ U [37] to implement a new density functional for the inter-site Coulomb interaction of V . With this, we achieve excellent agreements between the self-consistent *ab initio* band gaps of diverse semiconductors and insulators and those from experiments. The band gaps comparable to those from GW methods [24, 25] can be obtained within the standard DFT-GGA computational time. Moreover, for low dimensional systems in which the screening of Coulomb interaction varies significantly, the new method can also compute the accurate band gaps of few layers black phosphorous and Si(111)-(2×1) surface, respectively, demonstrating its flexibility on structural

* E-mail: lshgoal@kias.re.kr

† E-mail: hand@kias.re.kr

and dimensional variations. Considering recent explosive expansion of data-driven materials researches using the DFT [6–17], the improved accuracy in DFT computations is of great importance in constructing useful and reliable databases of materials. Thus, we expect that this new approach could accelerate efficient high-throughput calculations with better accuracy for materials discovery.

This paper is organized as follows. We first introduce our formalism of the ACBN0-like functional for the intersite Hubbard interactions in Sec. II. Then, using the new method described in Sec. III, we present our computational results of energy band gaps of various three-dimensional solids in Sec. IV and those of low dimensional systems in Sec. V. Finally, we discuss several aspects of the new functional and conclude in Sec. VI.

II. FORMALISM

Let us first consider mean-field (MF) energy of the Coulomb interaction between electrons in a pair of atoms I and J with the HF approximation,

$$E_{\text{MF}} = \frac{1}{2} \sum_{IJ} \sum_{ij} \sum_{\sigma\sigma'} \langle \phi_i^I \phi_j^J | V_{ee} | \phi_i^I \phi_j^J \rangle \times \left(n_{ii}^{II\sigma} n_{jj}^{JJ\sigma'} - \delta_{\sigma\sigma'} n_{ij}^{IJ\sigma} n_{ji}^{JI\sigma'} \right). \quad (1)$$

In the abbreviated representation of pairwise HF energy in Eq. (1), the general occupation matrix is written as

$$n_{ij}^{IJ\sigma} \equiv n_{ij}^{I,n,l,J,n',l',\sigma} = \sum_{m\mathbf{k}} w_{m\mathbf{k}} f_{m\mathbf{k}} \langle \psi_{m\mathbf{k}}^\sigma | \phi_i^{I,n,l} \rangle \langle \phi_j^{J,n',l'} | \psi_{m\mathbf{k}}^\sigma \rangle, \quad (2)$$

where $f_{m\mathbf{k}}$ is the Fermi-Dirac function of the Bloch state $|\psi_{m\mathbf{k}}^\sigma\rangle$ with a spin σ of the m -th band at a momentum \mathbf{k} and $w_{m\mathbf{k}}$ is the \mathbf{k} -grid weight. The Löwdin orthonormalized atomic wavefunction ($|\phi_i^{I,n,l}\rangle$) is used as a projector for the localized atomic orbital having the principal, azimuthal, and angular quantum numbers of n , l , and i , respectively at an atom I . We will use a brief notation for atom I representing a specific principal and azimuthal quantum numbers of n and l of the I -th atomic element in a solid hereafter. We also note that the diagonal terms in Eq. (2) are the usual on-site occupations for DFT+ U . In Eq. (1), we neglect other small pairwise interactions, *e.g.*, the cross charge exchanges between neighbors [40], and discuss their effects in Appendix A and in the Table AI.

Assuming the effective interactions of $\langle V_{ee} \rangle$ in Eq. (1) are all equal to their atomic average [40], the rotationally invariant or angular momentum averaged form of E_{MF} can be written as $E_{\text{MF}} = E_{\text{Hub}} = E_U + E_V$ where E_U is for the case of $I = J$ and E_V for $I \neq J$. E_U is the well-known energy functional for U suggested by Dudarev *et al.* [42]. For $I \neq J$ case where atoms I and J locate at

different positions, respectively,

$$E_V = \frac{1}{2} \sum_{\{I,J\}} \sum_{ij} \sum_{\sigma\sigma'} V^{IJ} \left(n_{ii}^{II\sigma} n_{jj}^{JJ\sigma'} - \delta_{\sigma\sigma'} n_{ij}^{IJ\sigma} n_{ji}^{JI\sigma'} \right), \quad (3)$$

where the $\{I, J\}$ indicates the summation for pairs of atoms I and J of which interatomic distance of d_{IJ} is less than a given cutoff. In Eq. (3), V^{IJ} is the inter-site Hubbard interaction for the pair and will be determined based on the method of ACBN0 [37].

To obtain a functional form of V^{IJ} , as is discussed for U in Ref. 37, we also follow a central ansatz by Mosey *et al.* [35, 36] that leads to a “renormalized” occupation number for the pair such as

$$\begin{aligned} N_{\psi_{m\mathbf{k}}}^{IJ\sigma} &\equiv N_{\psi_{m\mathbf{k}}}^{I,n,l,J,n',l',\sigma} \\ &= \sum_{\{I\}} \sum_i \langle \psi_{m\mathbf{k}}^\sigma | \phi_i^{I,n,l} \rangle \langle \phi_i^{I,n,l} | \psi_{m\mathbf{k}}^\sigma \rangle \\ &+ \sum_{\{J\}} \sum_j \langle \psi_{m\mathbf{k}}^\sigma | \phi_j^{J,n',l'} \rangle \langle \phi_j^{J,n',l'} | \psi_{m\mathbf{k}}^\sigma \rangle, \end{aligned} \quad (4)$$

where the summation performs for all the orbitals of a type I atom with quantum number n and l (denoted by $\{I\}$ in Eq. 4) and for a type J atom with n' and l' (denoted by $\{J\}$) in a given unit cell, respectively. Here we note that the sum is only obtained for all the given pairs within a specific distance. Therefore, we can obtain the ACBN0-like functional for V^{IJ} that effectively accounts the screening in the bond region between the pair, *e.g.*, the interaction between l -th orbital of I atom and l' -th orbital of J atom. Corresponding to the ACBN0 functional [37] for U , we can replace $n_{ij}^{IJ\sigma}$ in Eq. (1) by a renormalized density matrix for the pair,

$$P_{ij}^{IJ\sigma} = \sum_{m\mathbf{k}} w_{m\mathbf{k}} f_{m\mathbf{k}} N_{\psi_{m\mathbf{k}}}^{IJ\sigma} \langle \psi_{m\mathbf{k}}^\sigma | \phi_i^I \rangle \langle \phi_j^J | \psi_{m\mathbf{k}}^\sigma \rangle. \quad (5)$$

In case that there are no electrons participating the bond between atoms I and J , the renormalized density matrix of Eq. 5 for the pair automatically reduces to zero, thereby nullifying the inter-site effects. Note that I and J here also implicitly include orbital indexes.

The bare Coulomb interaction between electrons belong to the pair can be expressed by the electron repulsion integral [37],

$$V_{\text{ERI}} \equiv (ik|jl) \equiv \int d\mathbf{r}_1 d\mathbf{r}_2 \frac{\phi_i^{I*}(\mathbf{r}_1) \phi_k^I(\mathbf{r}_1) \phi_j^{J*}(\mathbf{r}_2) \phi_l^J(\mathbf{r}_2)}{|\mathbf{r}_1 - \mathbf{r}_2|}, \quad (6)$$

where i and k are orbital indices belong to atom I and j and l to atom J . Using Eqs (5) and (6), the ACBN0-like energy expression (E_{ACBN0}^V) for the inter-site Hubbard interaction can be written as

$$\begin{aligned} E_{\text{ACBN0}}^V &= \frac{1}{4} \sum_{\{I,J\}} \sum_{ijkl} \sum_{\sigma,\sigma'} \left[P_{ik}^{II\sigma} P_{jl}^{JJ\sigma'} - \delta_{\sigma\sigma'} P_{il}^{IJ\sigma} P_{jk}^{JI\sigma'} \right] \\ &\times (ik|jl), \end{aligned} \quad (7)$$

where the additional prefactor of $1/2$ arises from a double counting of the same pairs. Equating Eq. (3) to Eq. (7), then we can obtain a density functional form of V^{IJ} ,

$$V^{IJ} = \frac{1}{2} \frac{\sum_{\sigma,\sigma'} \sum_{ijkl} [P_{ik}^{II\sigma} P_{jl}^{JJ\sigma'} - \delta_{\sigma\sigma'} P_{ik}^{IJ\sigma} P_{jl}^{JI\sigma'}] (ik|jl)}{\sum_{\sigma,\sigma'} \sum_{ij} [n_{ii}^{II\sigma} n_{jj}^{JJ\sigma'} - \delta_{\sigma\sigma'} n_{ij}^{IJ\sigma} n_{ji}^{JI\sigma'}]}. \quad (8)$$

An energy functional for V can be constructed by subtracting a double counting term (E_V^{dc}) from E_V in Eq. (3). Following the discussion in Ref. 40, we use the fully localized limit and then $E_V^{\text{dc}} = \sum_{\{I,J\}} \sum_{i,j} \sum_{\sigma,\sigma'} \frac{V^{IJ}}{2} n_{ii}^{II\sigma} n_{jj}^{JJ\sigma'}$. With this, the final functional for the inter-site interaction of V can be written as

$$E_V[\{\mathbf{n}\}] = -\frac{1}{2} \sum_{\{I,J\}} \sum_{\sigma} V^{IJ}[\{\mathbf{n}\}] \text{Tr}[\mathbf{n}^{IJ\sigma} \mathbf{n}^{JI\sigma}], \quad (9)$$

where $\mathbf{n}^{IJ\sigma}$ is the matrix notation for the general occupation in Eq. (2), $\{\mathbf{n}\} = \{\mathbf{n}^{II\sigma}, \mathbf{n}^{JJ\sigma}\}$ and $V^{IJ}[\{\mathbf{n}\}]$ in Eq. (8). For the on-site repulsion, we used the ACBN0 functionals in Eqs (12) and (13) of Ref. 37 so that we complete a construction of the pseudohybrid-type functionals for the two essential Hubbard interactions. As discussed before [40], the minus sign in $E_V[\{\mathbf{n}\}]$ highlights the role of the inter-site Hubbard interaction that localizes electrons between atoms I and J . So, the equation (9) implemented in this study can improve the description of covalent bonding or augmenting the overlocalization [41] caused by U in case that the bonding between neighboring d - and p -orbitals plays important roles for the various ground state properties of solids.

III. COMPUTATIONAL METHODS

We implemented $E_V[\{\mathbf{n}\}]$ in Eq. (9), ACBN0 functionals and other related quantities in QUANTUM ESPRESSO package [43]. For the Kohn-Sham potential corresponding to Eq. (9), we used Eq. (13) in Ref. 40. To compute V_{ERI} in Eq. (6), we used the PAO-3G minimal basis set as in Ref. 37. With the aid of PyQuante package [44], the integrals were done quickly in an analytical way. For all calculations here, the cut-off for d_{IJ} sets within the second-nearest neighbors. We will discuss the effects of d_{IJ} later. The on-site interactions for s -orbitals were neglected for all materials considered here while for inter-site interaction, s -orbitals were included. Fully converged U and V were obtained when the difference in energy between two consecutive self-consistent steps is less than 10^{-8} Ry. We used the GBRV ultrasoft pseudopotentials [45]. Regarding pseudopotential dependence of ACBN0 functionals [38], we tested the norm-conserving pseudopotentials provided by PseudoDoJo project [46] and will discuss its effects in Appendix B. The kinetic energy cutoff was set to 160 Ry to fix the value for all materials. The Brillouin zone (BZ) integration was performed with a Γ -centered \mathbf{k} -point grid spacing of 0.2 \AA^{-1} .

The lattice structures are chosen from the experimentally available data for comparison to the results with other computational methods and otherwise are relaxed within a standard DFT scheme. For low dimensional materials discussed in Sec. V, we used slightly modified setups for computations and presented detailed methods in corresponding sections.

IV. ENERGY GAPS OF THREE DIMENSIONAL SOLIDS

We first tested our method for selected bulk solids with diverse characteristics. Table I and Fig. 1 summarize the calculated band gaps of 23 solids. We also listed the results from other calculations and measurements. We select solids from group IV, group III-V semiconductors, ionic insulators, metal chalcogenides and metal oxides. Our calculated band gaps are in excellent agreement with experiments and are as accurate as those from HSE and GW methods as shown in Table I. Mean absolute relative error (MARE) with respect to the experimental data indicates that our method, HSE and GW methods are closer to experiments than PBE and ACBN0. Mean relative error (MRE) shows that PBE and ACBN0 underestimate the gaps (minus sign) while GW method overestimates them. Hereafter, we mainly focus on the calculated gap values and, for future references, the band structures of all solids are displayed in Supplementary Information [59].

For the group IV semiconductors, the effect of U on the band gaps is almost negligible as shown in Table I (see ACBN0 column) while the inter-site Hubbard terms

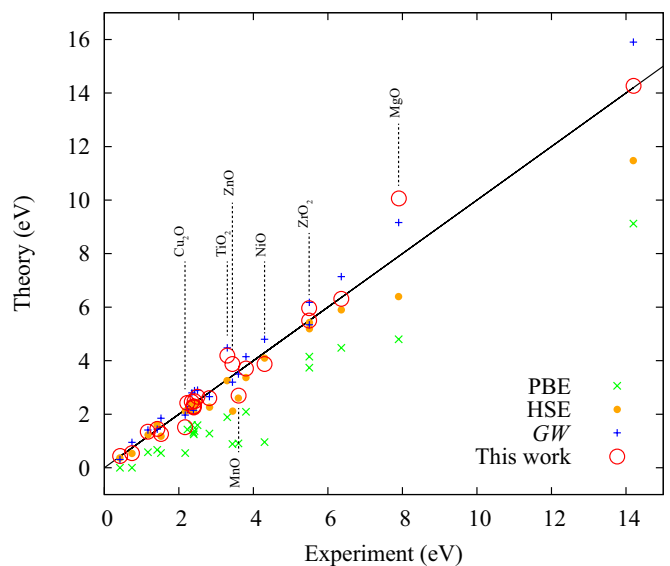


FIG. 1. Experimental versus theoretical band gaps in Table I. Metal oxides are marked and all other materials considered here are almost right on top of experimental values.

improve the band gaps dramatically as was also discussed in a previous study using the linear response theory [40].

For the group III-V semiconductors, both U and V affect their electronic structures because of their mixed covalent and ionic bonding characters. Therefore, ACBN0 improves the PBE gaps and the inter-site terms increases these further to match experiment values. Details of computations such as self-consistent U and V for Si and GaAs compared with Ref. 40 are discussed below. We note that PBE and ACBN0 incorrectly describe Ge and InAs as a metal and a topological insulator, respectively, while our method confirms them as semiconductors like HSE and

TABLE I. Calculated band gaps (in eV). For comparisons, gaps from experiments and other methods are also shown. Structures denoted by the Strukturbericht designation are in parenthesis. except monoclinic ZrO_2 . Experimental data are from Refs. 28, 29, 37, and 47 and references therein.

Solid	GGA ^a	ACBN0	This Work	HSE ^b	GW ^c	Expt.
C (A4)	4.15	4.17	5.50	5.43	6.18	5.50
Si (A4)	0.58	0.52	1.36	1.21	1.41	1.17
Ge (A4)	0.00	0.00	0.61	0.80	0.95	0.74
BP (B3)	1.25	1.24	2.27	2.13	2.20	2.40
AlP (B3)	1.59	2.00	2.66	2.42	2.90	2.50
GaP (B3)	1.60	1.74	2.47	2.39	2.80	2.35
InP (B3)	0.67	0.94	1.46	1.77	1.44	1.42
AlAs (B3)	1.43	1.75	2.43	2.13	2.18	2.23
GaAs (B3)	0.55	0.68	1.28	1.11	1.85	1.52
InAs (B3)	0.00	0.00	0.46	0.57	0.31	0.42
SiC (B3)	1.37	1.74	2.49	2.32	2.88	2.42
BN (B3)	4.48	5.14	6.31	5.91	7.14	6.36
ZnS (B3)	2.09	3.43	3.71	3.44	4.15	3.80
ZnSe (B3)	1.28	2.32	2.60	2.38	2.66	2.82
ZnTe (B3)	1.31	1.99	2.30	2.34	2.15	2.39
LiF (B1)	9.12	13.74	14.26	13.28	15.90	14.20
MgO (B1)	4.80	8.84	10.06	6.59	9.16	7.90
ZrO ₂ ^d	3.74	5.10	5.97	5.20	5.34	5.50
TiO ₂ (C4)	1.89	3.02	4.18	3.25	4.48	3.30
MnO (B1)	0.91	2.56	2.73	4.77	3.50	3.60
NiO (B1)	0.96	3.70	3.90	4.09	4.80	4.30
ZnO (B4)	0.89	3.62	3.88	2.11	3.80	3.44
Cu ₂ O (C3)	0.55	1.28	1.52	2.02	1.97	2.17
MARE (%)	52.71	30.26	10.64	11.83	13.62	
MRE (%)	-52.71	-28.78	0.47	-2.61	7.76	

^a GGA by Perdew-Burke-Ernzerhof (PBE) [4].

^b All data from HSE06 results in Ref. [48] except ZrO_2 from HSE06 in Ref. [49], TiO_2 from HSE03 in Ref. [50], ZnO from HSE03 in Ref. [51] and Cu_2O from HSE06 in Ref. [52]

^c All data from self-consistent GW (sc GW) calculation results in Ref. [25] except GaP, InP, AlAs from sc GW in Ref. [53], ZnSe from a partially self-consistent $GW(GW_0)$ in Ref. [54], BP from GW_0 in Ref. [55], ZrO_2 from sc GW in Ref. [56], TiO_2 from sc GW in Ref. [57], and Cu_2O from sc GW in Ref. [58].

^d Monoclinic structure

GW results.

We present the calculated U and V values for Si and GaAs to compare with the values obtained by the linear-response approach [40]. The Table II shows the calculated results. Our on-site U value for p -orbital of Si is larger than that reported in a previous study [40]. All the other inter-site terms except one between p -orbitals are smaller than those from the linear-response approach [40]. We note here that the on-site term for Si has no effect on the band gap at all. Despite of the differences in the Hubbard parameters, the calculated band gap of Si is in a good agreement with the previous linear response theory work [40] and experiment value. In case of GaAs, our on-site interactions for p -orbitals of Ga and As, respectively, are all smaller than the previous results [40]. Like Si case, our inter-site values are also smaller than the previous results except one between p -orbitals. Nevertheless, our computed band gap of 1.28 eV for GaAs is larger than the value of 0.90 eV reported in Ref. 40 and is close to the experimental gap of 1.52 eV (See Table I).

In case of ionic compound LiF, the on-site U improves the PBE band gap significantly because of its strong local Coulomb repulsion. Nonetheless, the inter-site V still increases the ACBN0 gap further to match with an experimental value.

A similar trend is also found in metal monochalcogenides (here Zn compounds only). For these compounds, the U and V functionals play similar roles as they do for LiF so that our results with U and V are quite closer to experiment values than those with U only. We note that the calculated gaps depends on the choice of pseudopotential of Zn while there is no such dependence in cases of IV and III-V semiconductors. We will discuss this further for cases of metal oxides below.

Regarding metal oxides, our results agree with the calculations by other advanced methods. For TiO_2 , MnO , NiO and ZnO in Table I, our ACBN0 results already improves PBE gaps significantly, similar with previous studies [37, 38, 60] that calculated the detailed electronic

TABLE II. Calculated U and V between s - and p -orbitals of the first nearest neighbors of Si and GaAs (in eV). Here we compare our results with those based on the linear response theory (LRT). For GaAs, the first (second) U_p for on-site Hubbard interactions on Ga (As) p -orbital. V_{sp} (V_{ps}) corresponds to inter-site terms between Ga $s(p)$ -orbital and As $p(s)$ -orbital. V_{pp} denotes the inter-site interaction between Ga p -orbital and As p -orbital.

		U_p	V_{ss}	V_{sp}	V_{ps}	V_{pp}
Si	This work	3.50	0.90	0.72	0.72	1.85
	LRT ^a	2.82	1.40	1.36	1.36	1.34
GaAs	This work	0.37, 1.88	0.91	1.26	0.80	1.75
	LRT ^a	3.14, 4.24	1.75	1.76	1.68	1.72

^a Reference 40

structures with ACBN0. Our gaps are slightly larger than the values in other works [37, 38, 60]. This discrepancies originate from the different self-consistent U values. With the inter-site V included, the changes in the on-site U lead to increase in the ACBN0 gaps of TiO_2 , MnO , ZnO and NiO as shown in Table III. We note that the gaps of metal oxides depend on the choice of pseudopotentials. With the potentials from the PseudoDoJo project [46], we achieve a better agreement (Table AII in Appendix). Because effects of on-site and inter-site interactions depend on degree of localization or cut-off in projector for localized orbital [38], it is important to select or generate pseudopotentials with care to obtain accurate results [61] or to develop a computational method for the on- and inter-site Hubbard interactions that do not depend on projectors.

For Cu_2O and Zr_2O , our results are comparable to those from HSE and GW calculations. We note here that for Cu_2O the calculated energetic position of fully filled d -orbitals is lower than that of HSE value [52] by ~ 0.9 eV [Fig. S7 in SI]. Since the degree of screening depends on occupancy of orbitals in the ACBN0 formalism, the weak screening for the fully filled d -orbitals like cuprite seems to be inevitable. Thus, it needs to improve the way to treat the completely filled d -orbitals with U and V within this formalism. Regardless of its limitation, we found that our computed gaps with V are considerably improved if compared with those from ACBN0 and mBJLDA. Considering limits in mBJLDA to obtain gaps for these compounds [29], our method could be a good alternative tool for studying zirconia and cuprite.

To compare with the previous ACBN0 studies on metal oxides [37, 38], we consider the on-site Hubbard interaction of U_d for d electrons of metals and U_p for p electrons of oxygen in TiO_2 , MnO , NiO and ZnO , respectively. We also provide those values and the first-nearest neighbor inter-site Hubbard interaction terms (the d - p interactions) calculated with our method. The results are summarized in Table III. We note that except TiO_2 our on-site repulsions for d -orbitals of metals are rather larger than the values from the previous works [37, 38] while the repulsions for oxide p orbitals are similar with the previous studies. Since the size of on-site repulsion of d -orbital is almost proportional to the size of gap, our larger estimations of U_d result in relatively larger direct energy gaps for MnO , NiO and ZnO , respectively if compared with the previous studies [37, 38]. With including the inter-site V_{dp} , the gaps increase further because of reduction in energetic position of conduction band maximum at Γ -point (See Figs. 6S in SI). As mentioned in Ref. 38, the discrepancies of U_d , U_p and E_g may be attributed to the way to calculate Coulomb integrals and the treatment of the localized orbitals. As shown in Table AII, our gap values also change according to the different choice of pseudopotentials. Therefore, a further study on this problem is required to obtain better description of electronic structures of metal oxides.

V. ENERGY GAPS IN LOW-DIMENSIONAL MATERIALS

Now, we consider low-dimensional systems where the screening of Coulomb interaction varies rapidly. The GW approximation calculates quasiparticle gaps quite accurately but its convergence is very slow with respect to the \mathbf{k} -points density and other parameters [62, 63]. The hybrid functional methods do not suffer such an issue but they produce unreliable gap values with structural or dimensional variations [64]. The mBJLDA, another low-cost alternative for bulk solids, also suffer a similar problem as hybrid functionals [65]. However, with our method, self-consistently computed occupations of atoms at boundary and bulk reflect the screening of Coulomb interaction through Eqs. (4), (5) and (8). Hence, we expect that the current method may overcome the aforementioned difficulties for low dimensional materials.

To test the new method, we first calculated the electronic structures of $\text{Si}(111)\text{--}(2 \times 1)$ surface. Because of a unique surface reconstruction resulting in a quasi-one-dimensional π -bonded chain of Si p_z -orbitals [68] and a large difference between the screenings on surface and in bulk, it is a good test bed for a method to compute surface and bulk gap simultaneously [64, 69]. A 24-layer slab

TABLE III. Self-consistent on-site energies of $3d$ orbitals of transition metal (U_d) and $2p$ orbitals of oxygen (U_p) and direct band gaps (E_g) of selected transition metal oxides within the ACBN0 formalism (in eV). We also list the self-consistent on-site and inter-site Hubbard interactions (V_{dp}) between the metal d and oxide p orbitals, and E_g using the current method.

Solids		U_d	U_p	V_{dp}	E_g
TiO_2	This work ^a	0.27	8.49		3.02
	ACBN0 ^b	0.15	7.34		2.83
	ACBN0 ^c	0.96	10.18		3.21
	This work ^d	0.37	8.21	2.94	4.18
MnO	This work ^a	5.11	2.99		3.05
	ACBN0 ^b	4.67	2.68		2.83
	ACBN0 ^c	4.68	5.18		2.65
	This work ^d	5.31	2.94	2.72	3.60
NiO	This work ^a	8.22	2.83		4.66
	ACBN0 ^b	7.63	3.00		4.29
	ACBN0 ^c	6.93	2.68		4.14
	This work ^d	7.77	2.37	2.93	5.13
ZnO	This work ^a	15.06	7.30		3.62
	ACBN0 ^b	12.80	5.29		2.91
	ACBN0 ^c	13.30	5.95		3.04
	This work ^d	14.96	7.07	3.01	3.88

^a DFT+ U

^b Reference 37

^c Reference 38

^d DFT+ U + V

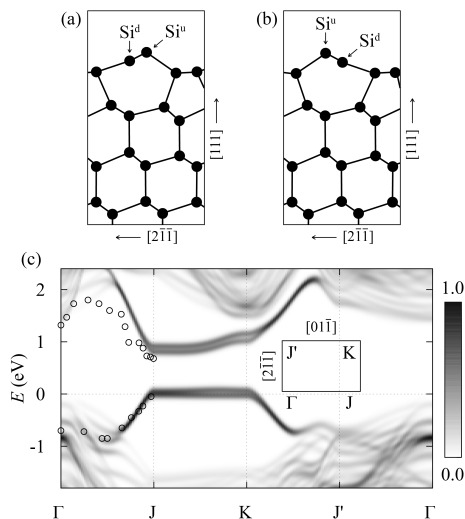


FIG. 2. The cross-sectional view of optimized atomic structures for two energetically degenerate buckled structures are shown in (a) and (b). Si atom (filled circles) relaxed down to (up away from) the surface is denoted by Si^d and Si^u, respectively. (c) Averaged surface band structures projected to the first four layers of Si(111)-(2 × 1) where the scale on the right side denotes local density of states in an arbitrary unit. The energetic position of bulk valence band maximum at Γ is set to zero. Black open circles are experimental data from direct [66] and inverse [67] photoemission spectroscopies experiments. The inset describes the BZ.

with ~ 15 Å vacuum was optimized with GGA until the residual forces on atoms are less than 10^{-4} Ry/Å. The kinetic energy cutoff is set to 80 Ry and d_{IJ} to the nearest neighbors. The surface has two degenerate and coexisting reconstructions [70, 71] as shown in Figs. 2 (a) and (b) so that we compute the averaged surface band structures to compare with experiments. As shown in Fig. 2 (c), the calculated averaged surface gap is 0.83 eV, agreeing well with the experimental value of 0.75 eV [66, 67], together with an accurate bulk gap. We note that the converged Hubbard parameters of Si atoms change spatially, reflecting the local variation of screening such that the calculated U and V are confirmed to gradually increase from inside to the surface (not shown here).

Next, few-layer black phosphorus (BP) was chosen to test our method [Fig. 3]. We used fully relaxed crystal structures using the rev-vdW-DF2 functional [75, 76]. All inter-site interactions between valence s and p electrons of P atom within the plane are considered. Fig. 3 shows the calculated band gaps in terms of the number of layers, together with other calculations and experiment. It is noticeable that, without including V , all ACBN0 gaps are quite smaller than GW gaps, and that HSE [65], mBJLDA [65] and ACBN0 produce the gaps close to the optical gaps by GW -BSE method [73]. Considering qualitative difference in shape of optical spectrum between GW -BSE and HSE or other hybrid functionals [64, 77],

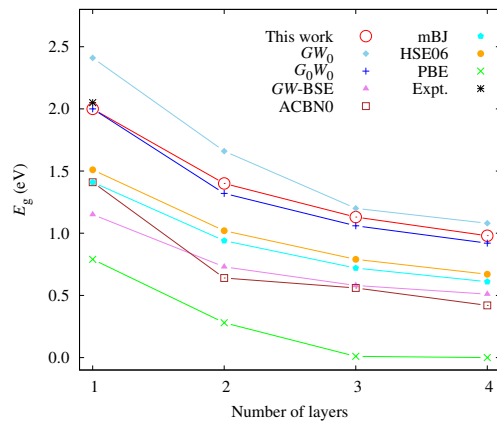


FIG. 3. Band gaps of black phosphorus as a function of a number of layers. We also list other gaps from PBE, HSE06 [65], mBJLDA [65], GW_0 [72], G_0W_0 [73] and GW -BSE [73]. A experimental band gap [74] is denoted with a black cross.

we conclude that they underestimate band gaps.

As shown in Fig. 3, our results are consistent with GW results [72, 73] and an available experiment [74]. We note that the computed band gaps of pure 2D materials such as single layer BP have a slight dependence on the range of inter-site Hubbard interaction (will be discussed in the next Section), reflecting complex nature of screening in low dimensional materials [62]. Considering a large number of atoms in typical nanostructures, our new method will have a merit over the other computational methods that requires quite expensive computational resources.

VI. DISCUSSION AND CONCLUSION

The only empirical parameter in the present formalism is d_{IJ} that determines the range of a pair for the inter-site V in Eqs. (3) and (9). For the three dimensional (3D) solids studied here, we find that the nearest neighbor inter-site interaction is enough to obtain the converged band gap values. As shown in Fig. 4, the energy band gap of 3D Si, GaAs and MnO crystals show a negligible variation as increasing d_{IJ} while the zincblende structure BN shows a converged gap after including the second nearest neighbors. Unlike the most 3D cases, the energy gaps for some low dimensional systems show rather larger variations as a function of d_{IJ} than 3D materials do. For the case of the reconstructed Si(111)-(2 × 1) surface discussed in the previous section, we don't need to include an inter-site V for the next nearest neighboring Si atoms. However, for a single layer BP shown in Fig. 4, the gap with V for the nearest neighbors is smaller (about 10%) than one with V for the next ones. Beyond this, the gap varies a little so that at least two sets of V with different d_{IJ} are required to obtain a reasonably converged band gap of the single layered BP. We note here that

TABLE IV. Calculated magnetic moments in μ_B of antiferromagnetic MnO and NiO and their comparisons with other works and experiments. Here the moments are projected values for one spin orientation.

	MnO	NiO
This work (+ V)	4.69	1.78
HSE [78]	4.5	1.5
ACBN0-PBE [60]	4.79	1.83
Experiments	4.58 [79], 4.79 [80]	1.77 [80], 1.90 [79, 81]

the increase in computational time with a longer d_{IJ} is amount to the increase in the DFT-GGA computation for a corresponding larger supercell case.

The role of self-consistent inter-site Hubbard interactions on magnetic moments is also an interesting issue. For this, we calculated magnetic moments of antiferromagnetic MnO and NiO. As shown in Table IV, the calculated magnetic moments are slightly reduced from the values using ACBN0-PBE method [60] where the on-site U enhance the localization of electrons at atomic sites. On the other hand, the inter-site V reduces the on-site localization and shifts electrons to the bonding sites. Therefore, the competition between U and V gives rise to the reduced magnetic moments compared with ACBN0 method and the calculated moments are in excellent agreement with experiments [79–81].

In conclusion, we report a new *ab initio* method for electronic structures of solids employing a pseudohybrid density functional for extended Hubbard Coulomb interactions. We demonstrate that the new method significantly improves the original ACBN0 functional in obtaining band gaps of bulk and low dimensional mate-

rials. Its self-consistent calculation can be done with a computational time comparable to DFT-GGA. With further validations with other methods [82, 83] and improvements of the current method such as the noncollinear spin and forces [38], our new method could fulfill requirements [6] for first-principles simulations suitable for massive database-driven materials research with an improved accuracy.

ACKNOWLEDGMENTS

We thank B.-H. Kim, H.-J. Kim, S.-H. Kang, S. Kim, S. Y. Park, S.-H. Jhi, H. J. Choi and M. J. Han for fruitful discussions. Y.-W.S was supported by NRF of Korea (Grant No. 2017R1A5A1014862, SRC program: vd-WMRC center) and KIAS individual grant (CG031509). Computations were supported by the CAC of KIAS. This work was also supported by the National Supercomputing Center with supercomputing resources including technical support (KSC-2018-C2-0017).

Appendix A: Effects of cross exchange interactions between orbitals

The mean-field (MF) expression of the electronic interaction energy in terms of atomic orbitals in its most general form can be written as ,

$$E_{\text{MF}} = \frac{1}{2} \sum_{I,J,K,L} \sum_{ijkl} \sum_{\sigma\sigma'} E_{ijkl,\sigma\sigma'}^{IJKL}, \quad (\text{A1})$$

where,

$$E_{ijkl,\sigma\sigma'}^{IJKL} = \langle \phi_i^I \phi_j^J | V_{ee} | \phi_k^K \phi_l^L \rangle \times \left(n_{ki}^{KI\sigma} n_{lj}^{LJ\sigma'} - \delta_{\sigma\sigma'} n_{kj}^{KJ\sigma} n_{li}^{LI\sigma'} \right), \quad (\text{A2})$$

where $n_{ij}^{IJ\sigma}$ is defined in Eq. (2).

Considering $E_{ijkl,\sigma\sigma'}^{IJKL}$, there are many possible arrangements for $IJKL$ and $ijkl$ [40], respectively. Among them, here we consider the first three large contributions, $E_{ijij,\sigma\sigma'}^{IIII}$, $E_{ijij,\sigma\sigma'}^{IJJJ}$ and $E_{ijji,\sigma\sigma'}^{IJJJ}$ where $I \neq J$. The first and second terms were discussed in the main manuscript and corresponds to the on-site and the inter-site Hubbard interactions, respectively. The last one is the cross charge exchanges between the neighboring atoms I and J [40]. The first case where all $IJKL$ are equals will lead to the well known Hubbard density functional for LDA+ U method and if we use a rotationally invariant on-site interaction (E_U^I), the Eq. (A1) will become to be Dudarev U functional [42]. The second term becomes the inter-site Hubbard interaction as discussed in the main manuscript.

Now, we consider the second and third ones together. If we use rotationally invariant forms for $\langle \phi_i^I \phi_j^J | V_{ee} | \phi_k^K \phi_l^L \rangle$ in Eq. (A2), we can rewrite the second

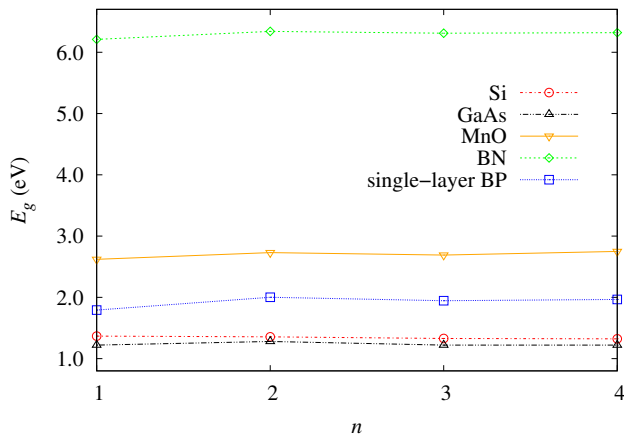


FIG. 4. Energy gap variations of Si, GaAs, MnO, BN and a single layer BP as a function of the distance between the pair atoms for the inter-site Hubbard interaction. The abscissa denotes n -th nearest neighbor and the ordinate shows the gap with including V 's up to the n -th neighbor.

interaction using $\langle \phi_i^I \phi_j^J | V_{ee} | \phi_k^K \phi_l^L \rangle = V^{IJ} \delta_{IK} \delta_{JL} \delta_{ik} \delta_{jl}$ and $N^{IJ} V^{IJ} = \sum_{i,j} \langle \phi_i^I \phi_j^J | V_{ee} | \phi_i^I \phi_j^J \rangle$ where N^{IJ} is a number of degeneracy of angular momentum for atoms I and J [40]. Likewise, the third interactions, we can use $\langle \phi_i^I \phi_j^J | V_{ee} | \phi_k^K \phi_l^L \rangle = K^{IJ} \delta_{IL} \delta_{JK} \delta_{il} \delta_{jk}$ and $N^{IJ} K^{IJ} = \sum_{i,j} \langle \phi_i^I \phi_j^J | V_{ee} | \phi_j^J \phi_i^I \rangle$. With these considerations, the MF energy in Eq. (A1) can be written as

$$E_{\text{Hub}} = \frac{1}{2} \left[\sum_I E_U^I + \sum_{\{I,J\}} E_V^{IJ} + \sum_{\{I,J\}} E_K^{IJ} \right], \quad (\text{A3})$$

where the $\{I, J\}$ indicates the summation for a pair of atoms I and J within a given cut-off of d_{IJ} .

Using the matrix notations of $\mathbf{n}^{IJ} = \sum_{\sigma} \mathbf{n}^{IJ\sigma}$ and

$n^I = \sum_{\sigma} \sum_i n_{ii}^{II\sigma}$ for the general occupation in Eq. (2),

$$E_V^{IJ} + E_K^{IJ} = V^{IJ} \left[n^I n^J - \sum_{\sigma} \text{Tr}[\mathbf{n}^{IJ\sigma} \mathbf{n}^{JI\sigma}] \right] + K^{IJ} \left[\text{Tr}[\mathbf{n}^{IJ} \mathbf{n}^{JI}] - \sum_{\sigma} n^{I\sigma} n^{J\sigma} \right] \quad (\text{A4})$$

We assume the fully localized limit for double counting as was also discussed in a previous work [40] so that the

TABLE AI. Calculated band gaps (in eV) with and without the cross charge exchange in Eq. (A6). ‘+V’ column summarizes the band gap with V^{IJ} and without K^{IJ} while ‘+V_{eff}’ column with $V_{\text{eff}}^{IJ} = V^{IJ} - K^{IJ}$. Experimental data for energy gaps are from Refs. [28, 29, 37, 47, 84, 85].

Solid	ACBN0	This Work (+V)	This Work (+V _{eff})	GW ^a	Expt.
C (A4)	4.17	5.50	5.36	6.18	5.50
Si (A4)	0.52	1.36	1.24	1.41	1.17
Ge (A4)	0.00	0.61	0.48	0.95	0.74
BP (B3)	1.24	2.27	2.14	2.20	2.40
AlP (B3)	2.00	2.66	2.58	2.90	2.50
GaP (B3)	1.74	2.47	2.39	2.80	2.35
InP (B3)	0.94	1.46	1.41	1.44	1.42
AlAs (B3)	1.75	2.43	2.35	2.18	2.23
GaAs (B3)	0.68	1.28	1.21	1.85	1.52
InAs (B3)	0.00	0.46	0.41	0.31	0.42
SiC (B3)	1.74	2.49	2.39	2.88	2.42
BN (B3)	5.14	6.31	6.17	7.14	6.36
ZnS (B3)	3.43	3.71	3.68	4.15	3.80
ZnSe (B3)	2.32	2.60	2.57	2.66	2.82
ZnTe (B3)	1.99	2.30	2.28	2.15	2.39
LiF (B1)	13.74	14.26	14.22	15.90	14.20
MgO (B1)	8.84	10.06	9.93	9.16	7.90
ZrO ₂	5.10	5.97	5.95	5.34	5.50
TiO ₂ (C4)	3.02	4.18	4.16	4.48	3.30
MnO (B1)	2.56	2.73	2.71	3.50	3.60
NiO (B1)	3.70	3.90	3.80	4.80	4.30
ZnO (B4)	3.62	3.88	3.86	3.80	3.44
Cu ₂ O (C3)	1.28	1.52	1.50	1.97	2.17
MARE (%)	30.26	10.64	10.81	13.62	
MRE (%)	-28.78	0.47	-3.11	7.76	

^a All data from self-consistent GW (scGW) calculation results in Ref. [25] except GaP, InP, AlAs from scGW in Ref. [53], ZnSe from G_0W_0 in Ref. [54], ZrO₂ from scGW in Ref. [56], TiO₂ from scGW in Ref. [57], and Cu₂O from scGW in Ref. [58].

TABLE AII. Calculated band gaps (in eV) with two different sets of pseudopotentials. We tested GBRV ultrasoft pseudopotentials [45] and the norm-conserving pseudopotentials provided by PseudoDoJo project [46]. Two ‘V’ columns summarize the calculated band gaps with the current method. Experimental data for energy gaps are from Refs. [28, 29, 37, 47, 84, 85].

Solid	ACBN0 ^a	ACBN0 ^b	+V ^c	+V ^d	Expt.
C (A4)	4.21	4.17	5.54	5.50	5.50
Si (A4)	0.52	0.52	1.35	1.36	1.17
Ge (A4)	0.00	0.00	0.60	0.61	0.74
BP (B3)	1.24	1.24	2.27	2.27	2.40
AlP (B3)	1.99	2.00	2.66	2.66	2.50
GaP (B3)	1.78	1.74	2.47	2.47	2.35
InP (B3)	1.00	0.94	1.46	1.46	1.42
AlAs (B3)	1.76	1.75	2.43	2.43	2.23
GaAs (B3)	0.70	0.68	1.22	1.28	1.52
InAs (B3)	0.00	0.00	0.44	0.46	0.42
SiC (B3)	1.73	1.74	2.49	2.49	2.42
BN (B3)	5.21	5.14	6.39	6.31	6.36
ZnS (B3)	4.30	3.43	4.77	3.71	3.80
ZnSe (B3)	3.16	2.32	3.62	2.60	2.82
ZnTe (B3)	2.73	1.99	3.28	2.30	2.39
LiF (B1)	14.88	13.74	16.01	14.26	14.20
MgO (B1)	8.89	8.84	10.16	10.06	7.90
ZrO ₂	5.32	5.10	6.19	5.97	5.50
TiO ₂ (C4)	2.89	3.02	4.08	4.18	3.30
MnO (B1)	2.88	2.56	3.55	2.73	3.60
NiO (B1)	4.30	3.70	4.82	3.90	4.30
ZnO (B4)	4.38	3.62	4.91	3.88	3.44
Cu ₂ O (C3)	1.63	1.28	2.02	1.52	2.17
MARE (%)	29.04	30.26	14.06	10.64	
MRE (%)	-21.73	-28.78	9.51	0.47	

^a PseudoDoJo pseudopotential

^b GBRV ultrasoft pseudopotential

^c PseudoDoJo pseudopotential

^d GBRV ultrasoft pseudopotential

final expression for Hubbard pairwise energy is given by,

$$\begin{aligned}
& E_V^{IJ} + E_K^{IJ} - E_{dc} \\
&= -V^{IJ} \sum_{\sigma} \text{Tr}[\mathbf{n}^{IJ\sigma} \mathbf{n}^{JI\sigma}] + K^{IJ} \text{Tr}[\mathbf{n}^{IJ} \mathbf{n}^{JI}] \\
&\simeq -(V^{IJ} - K^{IJ}) \sum_{\sigma} \text{Tr}[\mathbf{n}^{IJ\sigma} \mathbf{n}^{JI\sigma}], \quad (\text{A5})
\end{aligned}$$

where we neglect $K^{IJ} \sum_{\sigma \neq \sigma'} \text{Tr}[\mathbf{n}^{IJ\sigma} \mathbf{n}^{JI\sigma'}]$ thanks to $V^{IJ} - K^{IJ} \gg K^{IJ}$.

If we compare Eq. (A5) with the inter-site Hubbard functional shown in Eq. (9) in the main manuscript, we immediately notice that a replacement of V^{IJ} by $V_{\text{eff}}^{IJ} = V^{IJ} - K^{IJ}$ is enough for including the effects of cross charge exchange between the pair of atoms I and J .

Now using Eqs. (4)-(6) in the main manuscript, a pseudohybrid or ACBN0-like functional expression for K^{IJ} can be obtained in a straightforward way and the final expression can be written as

$$K^{IJ} = \frac{1}{2} \frac{\sum_{\sigma, \sigma'} \sum_{ijkl} [\delta_{\sigma\sigma'} P_{ik}^{II\sigma} P_{jl}^{JJ\sigma'} - P_{il}^{IJ\sigma} P_{jk}^{JI\sigma'}] (il|jk)}{\sum_{\sigma\sigma'} \sum_{ij} [\delta_{\sigma\sigma'} n_{ii}^{II\sigma} n_{jj}^{JJ\sigma'} - n_{ij}^{IJ\sigma} n_{ji}^{JI\sigma'}]}. \quad (\text{A6})$$

The effects of cross exchange interactions on band gaps are summarized in Table S1. As shown in Table A1, the calculated band gaps with and without effects of K are negligible. For solids considered here, all computed gaps with K are little bit smaller than the gap without K .

Appendix B: Effects of choice of pseudopotentials

In this work, we used two kinds of pseudopotentials: PseudoDoJo norm-conserving [46] and GBRV ultrasoft [45] pseudopotentials. Table AII shows the effects of choice of pseudopotentials. Almost all s and p electron systems considered here are not affected by the choice. However, particularly, in the case of Zn compound, the discrepancies are quite large.

-
- [1] P. Hohenberg and W. Kohn, Inhomogeneous electron gas, *Phys. Rev.* **136**, B864 (1964).
 - [2] W. Kohn and L. J. Sham, Self-consistent equations including exchange and correlation effects, *Phys. Rev.* **140**, A1133 (1965).
 - [3] R. O. Jones, Density functional theory: Its origins, rise to prominence, and future, *Rev. Mod. Phys.* **87**, 897 (2015).
 - [4] J. P. Perdew, K. Burke, and M. Ernzerhof, Generalized gradient approximation made simple, *Phys. Rev. Lett.* **77**, 3865 (1996).
 - [5] S. Kümmel and L. Kronik, Orbital-dependent density functionals: Theory and applications, *Rev. Mod. Phys.* **80**, 3 (2008).
 - [6] S. Curtarolo, G. L. W. Hart, M. Buongiorno Nardelli, N. Mingo, S. Sanvito, and O. Levy, The high-throughput highway to computational materials design, *Nat. Mater.* **12**, 191 (2013).
 - [7] J. Greeley, T. F. Jaramillo, J. Bonde, I. Chorkendorff, and J. K. Nørskov, Computational high-throughput screening of electrocatalytic materials for hydrogen evolution, *Nat. Mater.* **5**, 909 (2006).
 - [8] S. Wang, Z. Wang, W. Setyawan, N. Mingo, and S. Curtarolo, Assessing the thermoelectric properties of sintered compounds via high-throughput *ab-initio* calculations, *Phys. Rev. X* **1**, 021012 (2011).
 - [9] L. Yu and A. Zunger, Identification of potential photovoltaic absorbers based on first-principles spectroscopic screening of materials, *Phys. Rev. Lett.* **108**, 068701 (2012).
 - [10] R. Armiento, B. Kozinsky, M. Fornari, and G. Ceder, Screening for high-performance piezoelectrics using high-throughput density functional theory, *Phys. Rev. B* **84**, 014103 (2011).
 - [11] G. Hautier, A. Miglio, G. Ceder, G.-M. Rignanese, and X. Gonze, Identification and design principles of low hole effective mass p -type transparent conducting oxides, *Nat. Comm.* **4**, 2292 (2013).
 - [12] K. Yim, Y. Yong, J. Lee, K. Lee, H.-H. Nahm, J. Yoo, C. Lee, C. Seong Hwang, and S. Han, Novel high- κ dielectrics for next-generation electronic devices screened by automated *ab initio* calculations, *NPG Asia Mater.* **7**, e190 (2015).
 - [13] N. Mounet, M. Gibertini, P. Schwaller, D. Campi, A. Merkys, A. Marrazzo, T. Sohier, I. E. Castelli, A. Cepellotti, G. Pizzi, and N. Marzari, Two-dimensional materials from high-throughput computational exfoliation of experimentally known compounds, *Nat. Nanotechnol.* **13**, 246 (2018).
 - [14] K. Yang, W. Setyawan, S. Wang, M. Buongiorno Nardelli, and S. Curtarolo, A search model for topological insulators with high-throughput robustness descriptors, *Nat. Mater.* **11**, 614 (2012).
 - [15] T. Zhang, Y. Jiang, Z. Song, H. Huang, Y. He, Z. Fang, H. Weng, and C. Fang, Catalogue of topological electronic materials, *Nature* **566**, 475 (2019).
 - [16] M. G. Vergniory, L. Elcoro, C. Felser, N. Regnault, B. A. Bernevig, and Z. Wang, A complete catalogue of high-quality topological materials, *Nature* **566**, 480 (2019).
 - [17] F. Tang, H. C. Po, A. Vishwanath, and X. Wan, Comprehensive search for topological materials using symmetry indicators, *Nature* **566**, 486 (2019).
 - [18] V. I. Anisimov, J. Zaanen, and O. K. Andersen, Band theory and Mott insulators: Hubbard U instead of Stoner I , *Phys. Rev. B* **44**, 943 (1991).
 - [19] V. I. Anisimov, F. Aryasetiawan, and A. I. Lichtenstein, First-principles calculations of the electronic structure

- and spectra of strongly correlated systems: the LDA+ U method, *J. Phys.: Condens. Matter* **9**, 767 (1997).
- [20] W. Metzner and D. Vollhardt, Correlated Lattice Fermions in $d = \infty$ Dimensions, *Phys. Rev. Lett.* **62**, 324 (1989).
- [21] A. Georges and G. Kotliar, Hubbard model in infinite dimensions, *Phys. Rev. B* **45**, 6479 (1992).
- [22] G. Kotliar, S. Y. Savrasov, K. Haule, V. S. Oudovenko, O. Parcollet, and C. A. Marianetti, Electronic structure calculations with dynamical mean-field theory, *Rev. Mod. Phys.* **78**, 865 (2006).
- [23] L. Hedin, New method for calculating the one-particle Green's function with application to the electron-gas problem, *Phys. Rev.* **139**, A796 (1965).
- [24] M. S. Hybertsen and S. G. Louie, Electron correlation in semiconductors and insulators: Band gaps and quasiparticle energies, *Phys. Rev. B* **34**, 5390 (1986).
- [25] M. Shishkin, M. Marsman, and G. Kresse, Accurate quasiparticle spectra from self-consistent GW calculations with vertex corrections, *Phys. Rev. Lett.* **99**, 246403 (2007).
- [26] J. Heyd, G. E. Scuseria, and M. Ernzerhof, Hybrid functionals based on a screened coulomb potential, *J. Chem. Phys.* **118**, 8207 (2003).
- [27] B. G. Janesko, T. M. Henderson, and G. E. Scuseria, Screened hybrid density functionals for solid-state chemistry and physics, *Phys. Chem. Chem. Phys.* **11**, 443 (2009).
- [28] F. Tran and P. Blaha, Accurate band gaps of semiconductors and insulators with a semilocal exchange-correlation potential, *Phys. Rev. Lett.* **102**, 226401 (2009).
- [29] D. Koller, F. Tran, and P. Blaha, Merits and limits of the modified Becke-Johnson exchange potential, *Phys. Rev. B* **83**, 195134 (2011).
- [30] H. J. Kulik, M. Cococcioni, D. A. Scherlis, and N. Marzari, Density functional theory in transition-metal chemistry: A self-consistent Hubbard U approach, *Phys. Rev. Lett.* **97**, 103001 (2006).
- [31] M. Cococcioni and S. de Gironcoli, Linear response approach to the calculation of the effective interaction parameters in the LDA+ U method, *Phys. Rev. B* **71**, 035105 (2005).
- [32] T. Miyake and F. Aryasetiawan, Screened coulomb interaction in the maximally localized Wannier basis, *Phys. Rev. B* **77**, 085122 (2008).
- [33] M. Aichhorn, L. Pourovskii, V. Vildosola, M. Ferrero, O. Parcollet, T. Miyake, A. Georges, and S. Biermann, Dynamical mean-field theory within an augmented plane-wave framework: Assessing electronic correlations in the iron pnictide LaFeAsO, *Phys. Rev. B* **80**, 085101 (2009).
- [34] T. Miyake, F. Aryasetiawan, and M. Imada, *Ab initio* procedure for constructing effective models of correlated materials with entangled band structure, *Phys. Rev. B* **80**, 155134 (2009).
- [35] N. J. Mosey and E. A. Carter, *Ab initio* evaluation of Coulomb and exchange parameters for DFT+ U calculations, *Phys. Rev. B* **76**, 155123 (2007).
- [36] N. J. Mosey, P. Liao, and E. A. Carter, Rotationally invariant *ab initio* evaluation of Coulomb and exchange parameters for DFT+ U calculations, *J. Chem. Phys.* **129**, 014103 (2008).
- [37] L. A. Agapito, S. Curtarolo, and M. Buongiorno Nardelli, Reformulation of DFT+ U as a pseudohybrid Hubbard density functional for accelerated materials discovery, *Phys. Rev. X* **5**, 011006 (2015).
- [38] N. Tancogne-Dejean, M. J. T. Oliveira, and A. Rubio, Self-consistent DFT+ U method for real-space time-dependent density functional theory calculations, *Phys. Rev. B* **96**, 245133 (2017).
- [39] V. I. Anisimov, I. S. Elfimov, N. Hamada, and K. Terakura, Charge-ordered insulating state of Fe₃O₄ from first-principles electronic structure calculations, *Phys. Rev. B* **54**, 4387 (1996).
- [40] V. L. Campo Jr and M. Cococcioni, Extended DFT+ U + V method with on-site and inter-site electronic interactions, *J. Phys.: Condens. Matter* **22**, 055602 (2010).
- [41] H. J. Kulik and N. Marzari, Transition-metal dioxides: A case for the intersite term in Hubbard-model functionals, *J. Chem. Phys.* **134**, 094103 (2011).
- [42] S. L. Dudarev, G. A. Botton, S. Y. Savrasov, C. J. Humphreys, and A. P. Sutton, Electron-energy-loss spectra and the structural stability of nickel oxide: An LSDA+ U study, *Phys. Rev. B* **57**, 1505 (1998).
- [43] P. Giannozzi, S. Baroni, N. Bonini, M. Calandra, R. Car, C. Cavazzoni, D. Ceresoli, G. L. Chiarotti, M. Cococcioni, I. Dabo, A. D. Corso, S. de Gironcoli, S. Fabris, G. Fratesi, R. Gebauer, U. Gerstmann, C. Gougoussis, A. Kokalj, M. Lazzeri, L. Martin-Samos, N. Marzari, F. Mauri, R. Mazzarello, S. Paolini, A. Pasquarello, L. Paulatto, C. Sbraccia, S. Scandolo, G. Sclauzero, A. P. Seitsonen, A. Smogunov, P. Umari, and R. M. Wentzcovitch, QUANTUM ESPRESSO: a modular and open-source software project for quantum simulations of materials, *J. Phys.: Condens. Matter* **21**, 395502 (2009).
- [44] R. P. Muller, *PyQuante 1.6.4: Python Quantum Chemistry*, <http://pyquante.sourceforge.net/>.
- [45] K. F. Garrity, J. W. Bennett, K. M. Rabe, and D. Vanderbilt, Pseudopotentials for high-throughput DFT calculations, *Comput. Mater.* **81**, 446 (2014).
- [46] M. van Setten, M. Giantomassi, E. Bousquet, M. Verstraete, D. Hamann, X. Gonze, and G.-M. Rignanese, The pseudodojo: Training and grading a 85 element optimized norm-conserving pseudopotential table, *Comput. Phys. Commun.* **226**, 39 (2018).
- [47] M. J. Lucero, T. M. Henderson, and G. E. Scuseria, Improved semiconductor lattice parameters and band gaps from a middle-range screened hybrid exchange functional, *J. Phys.: Condens. Matter* **24**, 145504 (2012).
- [48] A. J. Garza and G. E. Scuseria, Predicting band gaps with hybrid density functionals, *J. Phys. Chem. Lett.* **7**, 4165 (2016).
- [49] J.-H. Yuan, Q. Chen, L. R. C. Fonseca, M. Xu, K.-H. Xue, and X.-S. Miao, GGA-1/2 self-energy correction for accurate band structure calculations: the case of resistive switching oxides, *J. Phys. Commun.* **2**, 105005 (2018).
- [50] H. Nakai, J. Heyd, and G. E. Scuseria, Periodic-boundary-condition calculation using Heyd-Scuseria-Ernzerhof screened Coulomb hybrid functional: electronic structure of anatase and rutile TiO₂, *J. Comput. Chem. Jpn.* **5**, 7 (2006).
- [51] F. Fuchs, J. Furthmüller, F. Bechstedt, M. Shishkin, and G. Kresse, Quasiparticle band structure based on a generalized Kohn-Sham scheme, *Phys. Rev. B* **76**, 115109 (2007).
- [52] M. Heinemann, B. Eifert, and C. Heiliger, Band structure and phase stability of the copper oxides Cu₂O, CuO, and Cu₄O₃, *Phys. Rev. B* **87**, 115111 (2013).

- [53] I. N. Remediakis and E. Kaxiras, Band-structure calculations for semiconductors within generalized-density-functional theory, *Phys. Rev. B* **59**, 5536 (1999).
- [54] Y. Hinuma, A. Grüneis, G. Kresse, and F. Oba, Band alignment of semiconductors from density-functional theory and many-body perturbation theory, *Phys. Rev. B* **90**, 155405 (2014).
- [55] H. Jiang and P. Blaha, *GW* with linearized augmented plane waves extended by high-energy local orbitals, *Phys. Rev. B* **93**, 115203 (2016).
- [56] H. Jiang, R. I. Gomez-Abal, P. Rinke, and M. Scheffler, Electronic band structure of zirconia and hafnia polymorphs from the *GW* perspective, *Phys. Rev. B* **81**, 085119 (2010).
- [57] S. Lany, Band-structure calculations for the 3d transition metal oxides in *GW*, *Phys. Rev. B* **87**, 085112 (2013).
- [58] F. Bruneval, N. Vast, L. Reining, M. Izquierdo, F. Sirotti, and N. Barrett, Exchange and correlation effects in electronic excitations of Cu_2O , *Phys. Rev. Lett.* **97**, 267601 (2006).
- [59] See Supplementary Information at <http://link.aps.org/supplemental>.
- [60] P. Gopal, R. D. Gennaro, M. S. dos Santos Gusmao, R. A. R. A. Orabi, H. Wang, S. Curtarolo, M. Fornari, and M. Buongiorno Nardelli, Improved electronic structure and magnetic exchange interactions in transition metal oxides, *J. Phys.: Condens. Matter* **29**, 444003 (2017).
- [61] H. J. Kulik and N. Marzari, A self-consistent Hubbard *U* density-functional theory approach to the addition-elimination reactions of hydrocarbons on bare FeO^+ , *J. Chem. Phys.* **129**, 134314 (2008).
- [62] D. Y. Qiu, F. H. da Jornada, and S. G. Louie, Screening and many-body effects in two-dimensional crystals: Monolayer MoS_2 , *Phys. Rev. B* **93**, 235435 (2016).
- [63] F. A. Rasmussen, P. S. Schmidt, K. T. Winther, and K. S. Thygesen, Efficient many-body calculations for two-dimensional materials using exact limits for the screened potential: Band gaps of MoS_2 , *h*-BN, and phosphorene, *Phys. Rev. B* **94**, 155406 (2016).
- [64] M. Jain, J. R. Chelikowsky, and S. G. Louie, Reliability of hybrid functionals in predicting band gaps, *Phys. Rev. Lett.* **107**, 216806 (2011).
- [65] J. Qiao, X. Kong, Z.-X. Hu, F. Yang, and W. Ji, High-mobility transport anisotropy and linear dichroism in few-layer black phosphorus, *Nat. Comm.* **5**, 4475 (2014).
- [66] R. I. G. Uhrberg, G. V. Hansson, J. M. Nicholls, and S. A. Flodström, Experimental evidence for one highly dispersive dangling-bond band on $\text{Si}(111)\text{-}2\times 1$, *Phys. Rev. Lett.* **48**, 1032 (1982).
- [67] P. Perfetti, J. M. Nicholls, and B. Reihl, Unoccupied surface-state band on $\text{Si}(111)\text{-}2\times 1$, *Phys. Rev. B* **36**, 6160 (1987).
- [68] K. C. Pandey, New π -bonded chain model for $\text{Si}(111)\text{-}2\times 1$ surface, *Phys. Rev. Lett.* **47**, 1913 (1981).
- [69] M. Rohlfling and S. G. Louie, Excitons and optical spectrum of the $\text{Si}(111)\text{-}2\times 1$ surface, *Phys. Rev. Lett.* **83**, 856 (1999).
- [70] K. Löser, M. Wenderoth, T. K. A. Spaeth, J. K. Garleff, R. G. Ulbrich, M. Pötter, and M. Rohlfling, Spectroscopy of positively and negatively buckled domains on $\text{Si}(111)\text{-}2\times 1$, *Phys. Rev. B* **86**, 085303 (2012).
- [71] C. Violante, L. Chiodo, A. M. Conte, F. Bechstedt, and O. Pulci, $\text{Si}(111)\text{-}2\times 1$ surface isomers: DFT investigations on stability and doping effects, *Surf. Sci.* **621**, 123 (2014).
- [72] V. Wang, Y. Kawazoe, and W. T. Geng, Native point defects in few-layer phosphorene, *Phys. Rev. B* **91**, 045433 (2015).
- [73] A. N. Rudenko, S. Yuan, and M. I. Katsnelson, Toward a realistic description of multilayer black phosphorus: From *GW* approximation to large-scale tight-binding simulations, *Phys. Rev. B* **92**, 085419 (2015).
- [74] L. Liang, W. Lin, B. G. Sumpter, V. Meunier, and M. Pan, Electronic bandgap and edge reconstruction in phosphorene materials, *Nano Lett.* **14**, 6400 (2014).
- [75] I. Hamada, van der waals density functional made accurate, *Phys. Rev. B* **89**, 121103 (2014).
- [76] H.-J. Kim, S.-H. Kang, I. Hamada, and Y.-W. Son, Origins of the structural phase transitions in MoTe_2 and WTe_2 , *Phys. Rev. B* **95**, 180101 (2017).
- [77] V. Tran, R. Soklaski, Y. Liang, and L. Yang, Layer-controlled band gap and anisotropic excitons in few-layer black phosphorus, *Phys. Rev. B* **89**, 235319 (2014).
- [78] C. Rödl, F. Fuchs, J. Furthmüller, and F. Bechstedt, Quasiparticle band structures of the antiferromagnetic transition-metal oxides MnO , FeO , CoO , and NiO , *Phys. Rev. B* **79**, 235114 (2009).
- [79] A. K. Cheetham and D. A. O. Hope, Magnetic ordering and exchange effects in the antiferromagnetic solid solutions $\text{Mn}_x\text{Ni}_{1-x}\text{O}$, *Phys. Rev. B* **27**, 6964 (1983).
- [80] B. E. F. Fender, A. J. Jacobson, and F. A. Wedgwood, Covalency parameters in MnO , $\alpha\text{-MnS}$, and NiO , *J. Chem. Phys.* **48**, 990 (1968).
- [81] W. L. Roth, Magnetic structures of MnO , FeO , CoO , and NiO , *Phys. Rev.* **110**, 1333 (1958).
- [82] J. Huang, S.-H. Lee, Y.-W. Son, A. Supka, and S. Liu, First-principles study of two-dimensional ferroelectrics using self-consistent Hubbard parameters, *Phys. Rev. B* **102**, 165157 (2020).
- [83] I. Timrov, N. Marzari, and M. Cococcioni, Self-consistent Hubbard parameters from density-functional perturbation theory in the ultrasoft and projector-augmented wave formulations (2020), arXiv:2011.03271 [cond-mat.mtrl-sci].
- [84] Y. Tezuka, S. Shin, T. Ishii, T. Ejima, S. Suzuki, and S. Sato, Photoemission and bremsstrahlung isochromat spectroscopy studies of TiO_2 (rutile) and SrTiO_3 , *J. Phys. Soc. Jpn.* **63**, 347 (1994).
- [85] G. A. Sawatzky and J. W. Allen, Magnitude and origin of the band gap in NiO , *Phys. Rev. Lett.* **53**, 2339 (1984).

Supplemental Material for “Efficient First-Principles Approach with a Pseudohybrid Density Functional for Extended Hubbard Interactions”

Sang-Hoon Lee and Young-Woo Son
Korea Institute for Advanced Study, Seoul 02455, Korea

In Figs. S1-S8, we displayed the band structures of selected bulk solids given in the main manuscript. In order to show the effects of inter-site interactions V on the band structures, we present the results obtained by DFT-PBE (Blue lines), ACBN0 method (gray dashed lines) and our method (red solid lines). The energetic position of valence band maximum is set to zero for all figures.

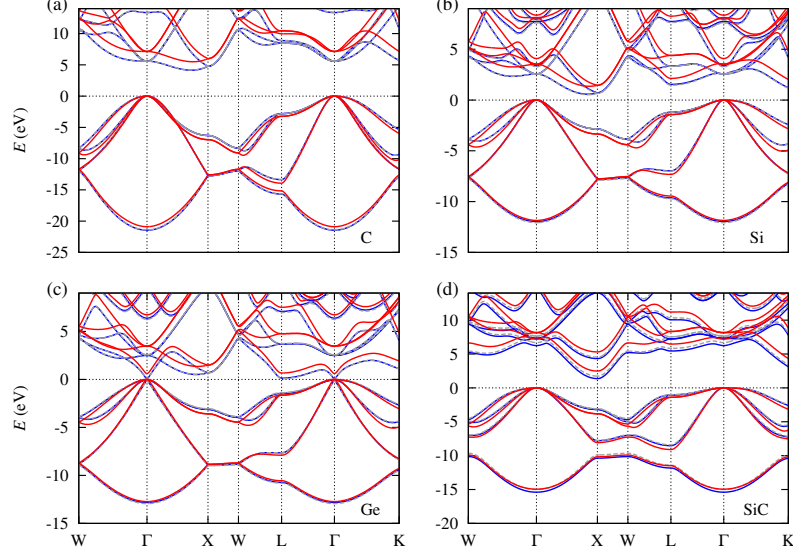


FIG. S1. Band structures of (a) C, (b) Si, (c) Ge, and (d) SiC

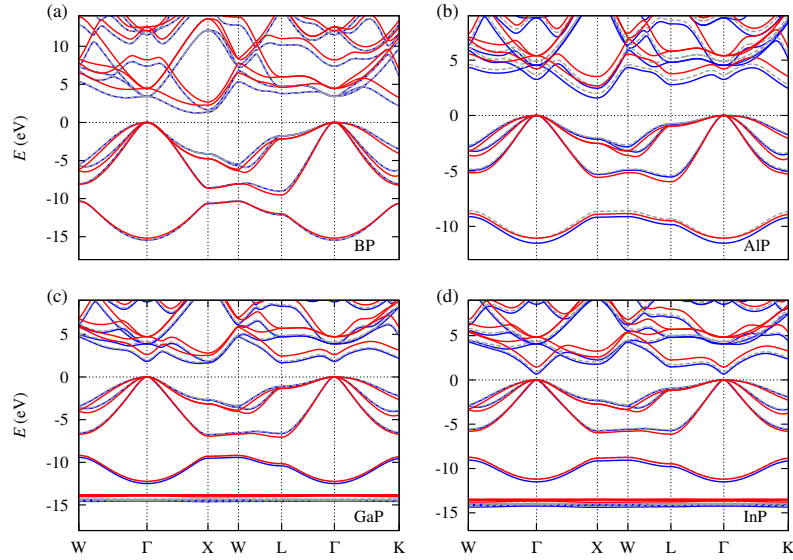


FIG. S2. Band structures of (a) BP, (b) AlP, (c) GaP, and (d) InP

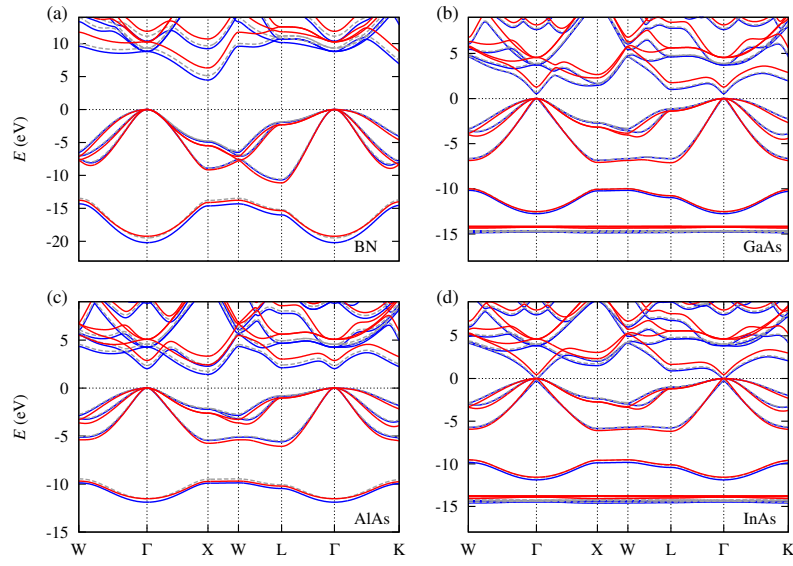


FIG. S3. Band structures of (a) BN, (b) GaAs, (c) AlAs, and (d) InAs

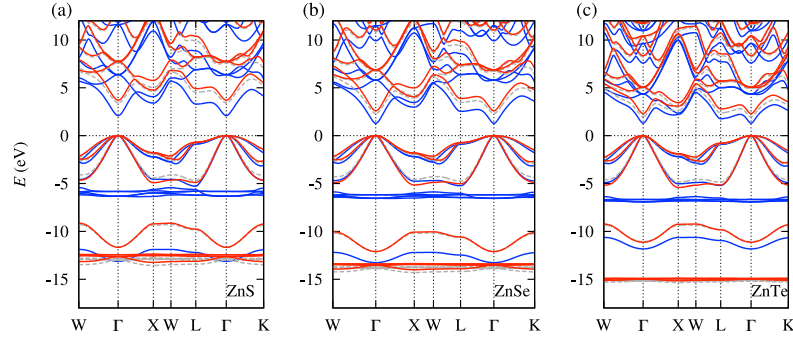


FIG. S4. Band structures of (a) ZnS, (b) ZnSe, and (c) ZnTe

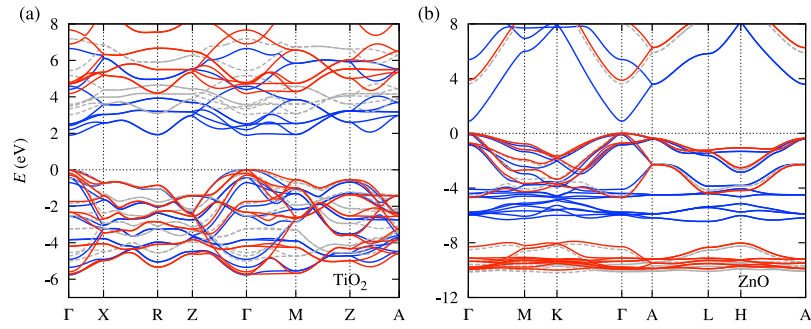


FIG. S5. Band structures of (a) TiO_2 , and (b) ZnO

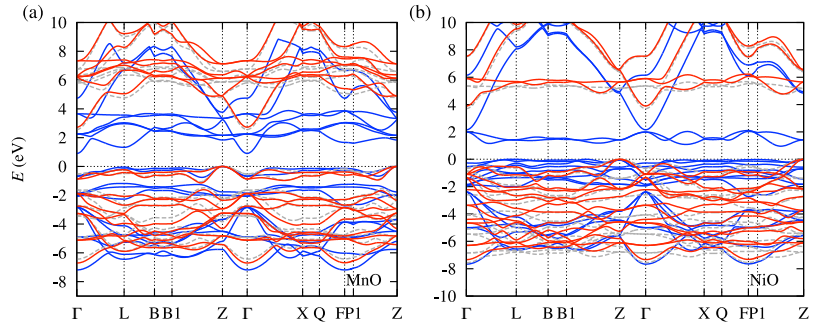


FIG. S6. Band structures of (a) MnO, and (b) NiO

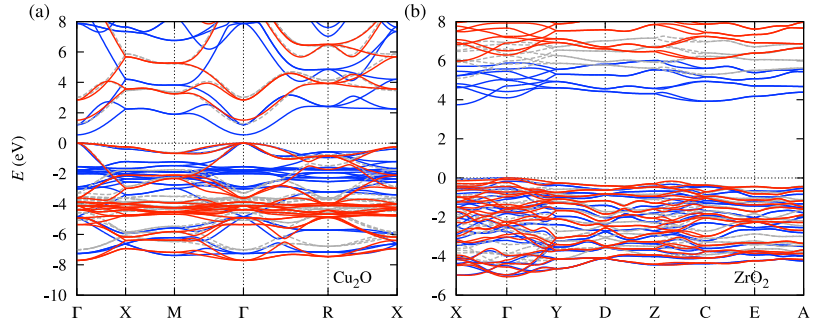


FIG. S7. Band structures of (a) Cu_2O , and (b) ZrO_2

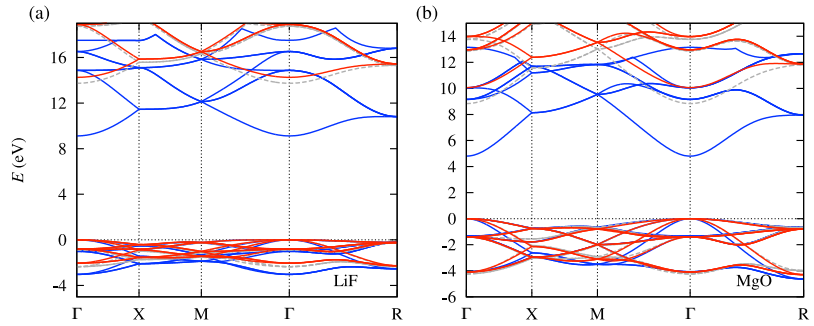


FIG. S8. Band structures of (a) LiF, and (b) MgO